

Alcohol extracts from *Anemone flaccida* Fr. Schmidt treat rheumatoid arthritis via inhibition of synovial hyperplasia and angiogenesis

QI RAO^{1*}, XIN ZHAO^{2*}, FENGHUA WU¹, XIAOHONG GUO¹, YUNDAN XU¹,
HE YU¹, DAYONG CAI² and GANG ZHAO¹

¹Department of Medical Biology, School of Basic Medical Sciences, Hubei University of Chinese Medicine, Wuhan, Hubei 430065; ²Institute of Medicinal Plant Development, Chinese Academy of Medical Sciences, Peking Union Medical College, Beijing 100193, P.R. China

Received October 13, 2022; Accepted February 22, 2023

DOI: 10.3892/mmr.2023.12975

Abstract. *Anemone flaccida* Fr. Schmidt, a Traditional Chinese Medicine, has been used in the treatment of rheumatoid arthritis (RA) for numerous years. However, the specific mechanisms remain to be elucidated. Thus, the present study aimed to investigate the main chemical constituents and potential mechanisms of *Anemone flaccida* Fr. Schmidt. The ethanol extract obtained from *Anemone flaccida* Fr. Schmidt (EAF) was analyzed using mass spectrometry to determine the main components and the therapeutic effects of EAF on RA were verified using a collagen-induced arthritis (CIA) rat model. Results of the present study demonstrated that synovial hyperplasia and pannus of the model rats were significantly improved following EAF treatment. Moreover, the protein expression levels of VEGF and CD31-labeled neovascularization were significantly reduced in the synovium of CIA rats following treatment with EAF, compared with those of the untreated model group. Subsequently, *in vitro* experiments were carried out to verify the impact of EAF on synovial proliferation and angiogenesis. Results of the western blot analysis revealed that EAF inhibited the PI3K signaling pathway in

endothelial cells, which is associated with anti-angiogenesis. In conclusion, results of the present study demonstrated the therapeutic effects of *Anemone flaccida* Fr. Schmidt on RA and preliminarily revealed the mechanisms of this drug in the treatment of RA.

Introduction

Rheumatoid arthritis (RA) is a common systemic inflammatory autoimmune disease that mainly affects human joints, manifesting as joint swelling, pain and deformation (1). RA affects ~1 in 200 adults worldwide and occurs 2-3 times more frequently in females than in males (2-4). It is characterized by tumor-like expansion of the synovium, angiogenesis and destruction of the adjacent articular cartilage and bone (5). Angiogenesis, a major component of invasive pannus, is considered an essential step in the abnormal proliferation of synovial cells and maintains a chronic inflammatory microenvironment by supplying oxygen and nutrients to tissues and recruiting immune cells (6,7). Disease-modifying antirheumatic drugs are the most well-established treatment option for RA. Immunosuppressants are the main choice of disease-modifying antirheumatic drug and may control symptoms in 40-50% of patients (8). Analgesics, such as non-steroidal anti-inflammatory drugs, may reduce joint pain in patients; however, these exert no effects on disease improvement (9). Moreover, clinical drug use may be limited due to associated adverse side effects (10). Thus, current research is focused on traditional herbal remedies for the treatment of RA (11,12), as novel therapeutic strategies for patients with RA are required.

Anemone flaccida Fr. Schmidt is mainly distributed in the mountainous areas of southern China. The dried rhizome, known as DIWU, is widely used as a Traditional Chinese Medicine (TCM) in the treatment of joint pain and fractures and the strengthening of bones (13). The main method of preparation of *Anemone flaccida* Fr. Schmidt for use in TCM includes decoction or soaking in wine. A previous pharmacological study demonstrated that the main components of triterpenoid saponins exhibit anti-inflammatory, anti-rheumatic and

Correspondence to: Professor Gang Zhao, Department of Medical Biology, School of Basic Medical Sciences, Hubei University of Chinese Medicine, 16 Huangjiahu West Road, Wuhan 430065, P.R. China
E-mail: zgcc66@163.com

Professor Dayong Cai, Institute of Medicinal Plant Development, Chinese Academy of Medical Sciences, Peking Union Medical College, 151, Malianwa North Road, Hai Dian, Beijing 100193, P.R. China
E-mail: dycai@implad.ac.cn

*Contributed equally

Key words: *Anemone flaccida* Fr. Schmidt, rheumatoid arthritis, synovial hyperplasia, angiogenesis, VEGF

anti-tumor properties (14). However, to the best of the authors' knowledge, there are no studies focusing on the potential of ethanol extract of *Anemone flaccida* Fr. Schmidt (EAF) in the treatment of RA. Thus, the present study aimed to explore the inhibitory effects of EAF on synovial hyperplasia and pannus formation in RA using a collagen-induced arthritis (CIA) rat model.

Materials and methods

EAF preparation. *Anemone flaccida* Fr. Schmidt used in the present study was collected from Yichang city (Hubei, China) and authenticated by Professor Keli-Chen (Department of Identification of Traditional Chinese Medicine, Hubei University of Chinese Medicine). The extraction method was as follows: *Anemone flaccida* Fr. Schmidt was dried and pulverized. A total of 500 g *Anemone flaccida* Fr. Schmidt powder was extracted twice using 500 ml absolute ethyl alcohol, following shaking in an incubator at 37°C for 24 h. The supernatant was collected following centrifugation (1,200 x g; 25°C) for 5 min, passed through filter paper and concentrated and dried via evaporation at room temperature for 48 h. Subsequently, 9.6 g of dry powder was extracted and the overall percentage of *Anemone flaccida* Fr. Schmidt was 1.92%. *Anemone flaccida* Fr. Schmidt was stored at -20°C for subsequent experiments.

Secondary metabolite detection. Sample extracts were analyzed using a UPLC-ESI-MS/MS system [UPLC: Shimadzu Corporation Nexera X2; MS: Applied Biosystems 4500 (AB4500) quadrupole-linear ion trap (QTRAP)]. The analytical conditions were as follows: Column, Agilent SB-C18 (1.8 µm, 2.1x100 mm); mobile phase, solvent A, pure water with 0.1% formic acid and solvent B, acetonitrile with 0.1% formic acid. Sample measurements were performed using a gradient program with 95% A and 5% B starting conditions. Within 9 min, a linear gradient to 5% A and 95% B was programmed and a composition of 5% A and 95% B was maintained for 1 min. Subsequently, a composition of 95% A and 5% B was adjusted within 1.1 min and maintained for 2.9 min. The flow velocity was set as 0.35 ml per minute; column oven was set to 40°C; and injection volume was set to 4 µl. The effluent was alternatively connected to an ESI-triple QTRAP-MS.

LIT and triple quadrupole (QQQ) scans were acquired on a QTRAP mass spectrometer, AB4500 QTRAP UPLC/MS/MS System, equipped with an ESI Turbo Ion-Spray interface, operating in positive and negative ion mode and controlled using Analyst 1.6.3 software (Shanghai AB SCIEX Analytical Instrument Trading Co.). ESI source operation parameters were as follows: Ion source, turbo spray; source temperature, 550°C; ion spray voltage (IS), 5,500 V (positive ion mode)/-4,500 V (negative ion mode); ion source gas I (GSI), 50 psi; gas II (GSII), 60 psi; curtain gas (CUR), 25.0 psi; and high collision-activated dissociation (CAD). Instrument tuning and mass calibration were performed using 10 and 100 µmol/l polypropylene glycol solutions in QQQ and LIT modes, respectively. QQQ scans were acquired as MRM experiments with collision gas (nitrogen) set to medium. DP and CE for individual MRM transitions were performed with further DP and CE optimization. A specific set of MRM transitions were

monitored for each period, according to the metabolites eluted within this period.

Animals. Animal experiments were carried out at the Animal Experiment Center of Hubei University of Chinese Medicine (registration no. syxk 2017-0067) following approval from the Hubei Experimental Animal Research Center (approval no. SCXK 2022-0012) and approval from the Laboratory Animal Ethics Committee of Hubei Academy of Chinese Medicine Sciences (approval no. HUCMS 202208001). Animal experimental procedures were in accordance with the National Regulations on the Management of Experimental Animals, Government of China. Male Wistar rats (age, 6-8 weeks; weight, 160±10 g; SPF grade; cat. no. 42000600043481) obtained from the Hubei Laboratory Animal Research Center were housed at 22±3°C, in 30-70% relative humidity, with a 12/12 h light/dark cycle. Standard rodent feed and water were provided for all animals *ad libitum*. Rats were fed for five days prior to the commencement of experimental procedures for acclimation.

Induction of arthritis and drug administration. The RA rat model was induced as previously described (15). Briefly, Bovine type II collagen (cat. no. 01025A; Dalian Meilun Biology Technology Co., Ltd.) was dissolved in 0.05 mol/l acetic acid (2.0 mg/ml) and emulsified with complete Freund's adjuvant (CFA; cat. no. F5881-10 ml; Sigma-Aldrich; Merck KGaA) at a ratio of 1:1. The prepared emulsifier was injected intradermally into the base of the rat tail at 100 µg per rat. A second immunization with the same dose was administered 7 days later. Redness and swelling of the ankle of the rats was observed and arthritis score was evaluated and recorded. Briefly, 15 days after the first immunization, outliers were excluded according to arthritis score. A total of 20 rats remained and these were randomly divided into four groups (5 rats in each group): i) CIA (200 mg/kg); ii) vehicle (200 mg/kg); iii) EAF-L (200 mg/kg); and iv) EAF-H (400 mg/kg). A further five rats that did not receive immunization were used as the blank control group. Notably, the body weight of all rats was recorded every 7 days.

From the 15th day, groups were treated as follows: i) Control and CIA groups, daily intraperitoneal injection of saline; ii) vehicle group, daily intraperitoneal injection of equal volume of DMSO; and iii) EAF group, daily intraperitoneal injection of EAF 200 or 400 mg/kg.

Following immunization, all four paws of the rats were observed and the arthritic condition was evaluated based on the redness and swelling every three days. Redness and swelling was scored according to the following criteria: 0, without redness and swelling; 1, localized redness or swelling (wrist/ankle); 2, swelling or redness expanded to the palm or sole; 3, redness and swelling in all joints; and 4, skin bursting, joint dysfunction or distortion. Clinical assessments were completed by two independent researchers. The sum of arthritis index scores in the limbs was used to evaluate the severity of arthritis, with higher scores indicating more severe arthritis. The humane endpoints in this experiment were based on the following criteria: No sign of healing after ulcer treatment, abnormal gait or posture that prevented them from feeding, spontaneous vocalization or squeaking and quivering when picked up or handled, significant weight loss (15%) (16).

Histological assessment. Rats were euthanized using an intra-peritoneal injection of sodium pentobarbital (3%; 100 mg/kg). Arthritis severity was assessed through observing inflammatory infiltration, pannus and synovial edema in samples obtained from the joints, following paraffin embedding and H&E staining. The right hindlimb was collected and fixed in 4% paraformaldehyde for 48 h at 4°C. Following two weeks of slow decalcification, the right hindlimb was embedded in paraffin and cut into 5- μ m thick sections. Subsequently, H&E staining was carried out according to standard protocols.

Parts of the sections were used for immunohistochemical examination and a CD31 antibody (1:200; cat. no. bs-0195R; BIOSS) was used measure neovascularization. A VEGF antibody (1:200; cat. no. bs-0279R; BIOSS) was used in sliced tissue. Primary antibody incubated for 12 h at 4°C, secondary antibody incubated for 2 h at room temperature. Stained or protein-labeled specimen slices were observed and a total of five fields of view were randomly selected and images captured using light microscopy (CH30RF200; Olympus Corporation) at a high magnification (x200 and x400). Positive expression of proteins was semi-quantified using ImageJ 1.8.0. (National Institutes of Health).

Rat aortic ring assay. Healthy 8-week-old male Wistar rats were euthanized using an intraperitoneal injection of sodium pentobarbital (3%; 100 mg/kg) and thoracic aorta segments were collected. Thoracic aorta segments were cleaned and cut into 1-mm long complete rings and placed in a 96-well plate pre-coated with Matrigel (Corning, Inc.) mixed with DMEM (HyClone; Cytiva) medium (1:1; 40 μ l/well). Subsequently, 200 μ l medium with 20% FBS (Hangzhou Sijiqing Biological Engineering Materials Co., Ltd.) was added in each well. The plate was incubated at 37°C with 5% CO₂ for 3 days until endothelial cells budded in tubular structures around the vascular ring. Vascular rings were divided into four groups with five in each group and VEGF and/or EAF was added in each group. Following incubation for a further seven days, the vascular sprout was observed and images captured using an inverted microscope (Eclipse TS 100; Nikon Corporation).

Chick chorioallantois membrane (CAM) assay. To explore the effects of EAF on angiogenesis in synovial tissues, a CAM model was used. Briefly, fertilized hen's eggs were incubated at 37.8°C and 60% relative humidity for five days. A total of 2 ml albumin was removed under aseptic conditions and placed in an artificial air chamber. Following two days incubation, 1-mm³ gelatin sponges soaked in basic medium, EAF and/or recombinant human VEGF165 protein (VEGF165; BIOSS) was placed on the CAM through a 1x1 cm² window, opened in the large blunt edge of the egg. Subsequently, the window was sealed using paraffin film for further incubation for three days. The microvasculature was observed and photographed under a dissecting microscope (XTL-165-XTWZ; Phenix Optics Co., Ltd.).

Cells and culture methods. Human umbilical vein endothelial cells (HUVECs; cat. no. C1109) and human fibroblast-like synoviocytes-RA (HFLS-RAs; cat. no. C1351) were purchased from Shanghai Whelab Biological Co., Ltd. Cells were cultured in DMEM (HyClone; Cytiva) containing 5% FBS

(Hangzhou Sijiqing Biological Engineering Materials Co., Ltd.) and 1% penicillin/streptomycin (Dalian Meilun Biology Technology Co., Ltd.) and cultured in a humid incubator at 37°C with 5% CO₂.

Cell viability assay. A Cell Counting Kit-8 (CCK-8) assay was used to detect the effects of EAF on the viability of HFLS-RAs and HUVECs. HFLS-RAs (3x10³ cells/ml) or HUVECs (5x10³ cells/well) were seeded in 96-well plates and cultured in normal growth medium for 24 h. Culture medium was replaced with DMEM, different concentrations (HUVEC: 5, 7.5, 10, 15, 20, 30 μ g/ml; HFLS-RA: 2.5, 5, 10, 20, 40, 80 μ g/ml) of EAF were added and cells were incubated for 24 or 48 h at 37°C. Following incubation, culture medium was replaced with 200 μ l PBS containing 10% CCK-8 (Dalian Meilun Biology Technology Co., Ltd.). Following a further 2 h incubation at 37°C, the viability of HFLS-RAs and HUVECs was measured at an absorbance of 490 nm using a microplate reader (Model 680; Bio-Rad Laboratories, Inc.). Cell viability was measured using the following formula: Inhibitory rate (%)=[(1-optical density at 450 nm of the treatment)/optical density at 450 nm of the control] x100%.

Wound healing assay. A wound healing assay was conducted in a six-well plates to determine the migration of HFLS-RAs. Cells were seeded and incubated in normal growth medium until 90% confluence was reached. The cell layer was scratched using a 200- μ l pipette tip. Following washing with PBS twice, 2 ml serum-free medium with different concentrations of EAF was added to each well and incubated for a further 24 h. Images were captured at 0 and 24 h and the start of the wound was marked with a marker under an inverted microscope (model CK-40; Olympus Corporation). Changes in wound width were calculated using ImageJ 1.8.0 (National Institutes of Health).

Migration assay. A Transwell assay was used to detect the vertical migration of HUVECs and HFLS-Ras (17). Transwell chambers with pore size 8.0 μ m were placed in 24-well plates and cells were seeded in the upper chamber at a density of 2x10⁵ cells/well. Cells were suspended in serum-free medium following treatment with EAF and/or VEGF165 in a six-well plate for 24 h at 37°C. The lower chamber was filled with 700 μ l medium and 10% FBS and incubated at 37°C for 12 h at 37°C. Subsequently, cells that failed to migrate to the lower layer were removed with a cotton swab and cells on the lower surface were fixed with anhydrous ethanol and stained with 0.5% crystal violet for 5 min at room temperature. The number of migratory cells in each well was counted in five random fields using an inverted microscope (model CK-40; magnification, x100; Olympus Corporation).

Cell colony formation assay. The effects of EAF on cell proliferation were detected using a colony formation assay. Briefly, HFLS-RAs were seeded in a six-well plate at a density of 500 cells/well and incubated for two days at 37°C. Following treatment with different concentrations of EAF for 12 h at 37°C, culture medium was replaced with complete medium. Subsequently, cells were incubated for a further two weeks at 37°C, colonies were fixed using anhydrous ethanol for 10 min at room temperature and stained using 0.5% crystal violet for

5 min at room temperature. The number of colonies (>50 cells) in each well was quantified using ImageJ 1.8.0. (National Institutes of Health).

Flow cytometry. A FITC-Annexin V/PI apoptosis kit was used to detect the apoptotic rate of HFLS-RAs following treatment with EAF. Cells were collected following treatment with different concentrations of EAF for 24 h and washed twice using cold PBS. FITC-Annexin V (5 μ l) and PI (10 μ l) were sequentially added to cells following resuspension in 400 μ l binding buffer. Cells were incubated in the dark for 15 min at room temperature, following detection using a BD FACSCalibur flow cytometer (BD Biosciences). The results were analyzed using FlowJo X 10.0.7 (FlowJo LLC), the apoptotic rate was calculated by the percentage of early + late apoptotic cells.

Tube formation assay. The formation of tubule-like structures by HUVECs in Matrigel may reflect their angiogenic capacity; thus, HUVECs were pre-treated with or without EAF and/or VEGF165 for 12 h at 37°C. Cells were resuspended in medium with various concentrations of EAF and/or VEGF165 and seeded in 96-well plate, which had been pre-coated with a 50 μ l layer of Matrigel. Following a further 12-h incubation at 37°C, images was captured under an inverted microscope (model CK-40; magnification, x40; Olympus Corporation). Tubular structures in five random fields of view were calculated using ImageJ 1.8.0 (National Institutes of Health).

Western blot analysis. HUVECs were seeded in a six-well plate and treated with different concentrations of EAF and/or VEGF165 for 24 h. Total protein was collected using RIPA lysis buffer (Beyotime Institute of Biotechnology) containing proteinase inhibitors. Proteins were quantified using BCA (Beyotime Institute of Biotechnology) and denatured using 5X loading buffer. A total of 20 μ g protein from each group was separated via SDS-PAGE using a 10% gel and transferred onto PVDF membranes. Following blocking with 5% skimmed milk at room temperature for 1 h, membranes were incubated with the following primary antibodies at 4°C for 12 h: Rabbit anti-VEGF antibody (1:1,000; cat. no. bs-0279R; BIOSS), anti-VEGF receptor (VEGFR)1 antibody (1:1,000; cat. no. bs-0170R; BIOSS), anti-PI3K antibody (1:1,000; cat. no. AF7742; Beyotime Institute of Biotechnology), anti-phosphorylated (p)-PI3K antibody (1:1,000; cat. no. AF5905; Beyotime Institute of Biotechnology), anti-AKT antibody (1:1,000; cat. no. AA326; Beyotime Institute of Biotechnology), anti-p-AKT1 antibody (1:1,000; cat. no. AF5740; Beyotime Institute of Biotechnology), anti-mTOR antibody (1:1,000; cat. no. AF1648; Beyotime Institute of Biotechnology), anti-p-mTOR antibody (1:1,000; AF5869; Beyotime Institute of Biotechnology). β -actin was used as the control and detected using the anti- β -actin antibody (1:1,000; cat. no. K200058M; Beijing Solarbio Science & Technology Co., Ltd). Following primary incubation, membranes were incubated with the anti-goat HRP-conjugated immunoglobulin G secondary antibody (1:1,000; cat. no. SE134; Beijing Solarbio Science & Technology Co., Ltd.) at room temperature for 2 h. Proteins were visualized using enhanced chemiluminescent reagent (Wuhan Servicebio Biotechnology Co., Ltd.) and membranes were scanned using a gel imaging

system (ChemiDoc XRS+; Bio-Rad Laboratories, Inc.). Protein expression was quantified using Image Lab software (version 5.0; Bio-Rad Laboratories, Inc.).

Statistical analysis. GraphPad Prism (version 8.00; GraphPad Software, Inc.) was used for statistical analysis. Data are presented as the mean \pm standard deviation. All experiments were repeated at least three times. One-way ANOVA followed by Tukey's post-hoc test was used for comparisons between multiple groups. $P < 0.05$ was considered to indicate a statistically significant difference.

Results

Qualitative chemical analysis using ultra-high-performance liquid chromatography–high-resolution tandem mass spectrometry (UHPLC-ESI-HRMS). UPLC-MS analysis of EAF was performed in the positive and negative ion mode. The UV detector and total ion chromatograms of EAF are displayed in Fig. 1. Through the chemical analysis of EAF, a total of six classes of metabolites were identified, including: Iridoids glycosides, flavonoids, phenylpropanoids-derived metabolites, phenylethanoid-derived metabolites, cinnamic acid-derived metabolites and triterpenes (Table I). Identification of the chemical substances in EAF were compared with the main chemical constituents of *Anemone* plants described in an internal database (18). The results of the phytochemical analysis were consistent with those of previous studies (13,19).

EAF reduces joint inflammation in CIA rats. Animals were treated on the 15th day following the first immunization and treatment lasted for 21 days. Joint inflammation clinical scores were recorded every three days and body weights of rats were recorded every seven days. Results are displayed in Fig. 2. The degree of limb swelling and redness in the EAF treatment group was significantly improved compared with the control groups. Notably, clinical scores were increased in vehicle and CIA groups and peaked 33 days following the first immunization with no significant difference between the two groups. Treatment groups were significantly different from the model group on day 21 and gradually decreased after peaking on day 24. Clinical scores were lower in the EAF-high (H) group than in the EAF-low (L) group and this gap was present on Day 9 and continued until the end of the experiment. Body weight is displayed in Fig. 2C. All immunized animals exhibited a significant reduction in body weight compared with the control group. Results of the present study demonstrated no difference between the EAF treatment group and the model group. In addition, results of H&E staining (Fig. 2E) demonstrated that the thickness of joint synovial tissue was lower in the EAF treatment group compared with the model group and notable pannus formation was present in the joints of animals in the model group. By contrast, pannus was significantly reduced or absent in the EAF-treated group.

EAF relieves joint synovial hyperplasia and pannus. H&E staining revealed that EAF treatment significantly reduced pannus formation in the joint synovium of arthritic rats. Given the important role of angiogenesis in RA progression, immunohistochemical staining was performed using joint tissue

Table I. Qualitative chemical analysis of extract of *Anemone flaccida* Fr. Schmidt by ultra-high-performance liquid chromatography-high-resolution tandem mass spectrometry.

Number	Retention time	Formula	Compound type	Ionization model	Putative compounds
1	1.45	C ₁₈ H ₂₆ O ₁₁	Phenolic acids	[M-H]-	2-Hydroxyphenol-1-O-glucosyl(6→1) rhamnoside
2	2.63	C ₁₄ H ₂₀ O ₉	Phenolic acids	[M-H]-	glucopyranoside
3	2.83	C ₂₇ H ₃₆ O ₁₃	Phenolic acids	[M-H]-	Citrusin B
4	3.61	C ₃₀ H ₃₈ O ₁₅	Phenolic acids	[M-H]-	Glucopyranosyl)-feruloyl]glucopyranoside
5	3.73	C ₃₁ H ₄₁ NO ₁₁	Terpenoid alkaloids	[M+H]+	Flavaconitine
6	3.92	C ₂₇ H ₃₀ O ₁₄	Flavonoids	[M+H]+	Apigenin-7-O-rutinoside (Isorhoifolin)
7	4.04	C ₂₉ H ₃₆ O ₁₅	Phenolic acids	[M-H]-	Acteoside
8	4.04	C ₂₉ H ₃₆ O ₁₅	Phenolic acids	[M-H]-	Isoforsythoside A
9	4.05	C ₂₈ H ₃₆ O ₁₃	Lignans	[M-H]-	Syringaresinol-4'-O-glucoside
10	4.48	C ₃₃ H ₄₅ NO ₁₁	Terpenoid alkaloids	[M+H]+	Mesaconitine
11	4.52	C ₃₂ H ₄₅ NO ₉	Terpenoid alkaloids	[M+H]+	Hemsleyaconitine B
14	4.68	C ₂₈ H ₃₂ O ₁₄	Flavonoids	[M+H]+	Robinson-7-O-Neohesperidin
15	6.24	C ₃₅ H ₅₄ O ₈	Terpenoids	[M+H]+	3β-[(Arabinosyl)oxy]-19β-hydroxyurs-12,20(30)-dien-28-oic acid
16	6.47	C ₃₃ H ₄₀ O ₁₄	Flavonols	[M+H]+	2'-O-rhamnosyl-icariside II
17	6.90	C ₃₀ H ₄₈ O ₄	Triterpene	[M+H]+	Hederagenin
18	9.66	C ₃₆ H ₅₆ O ₉	Terpenoids	[M+H]+	Oleanolic acid-GlurA
19	9.63	C ₃₀ H ₄₆ O ₃	Terpenoids	[M-H]-	Oleanonic acid
20	6.24	C ₄₁ H ₆₄ O ₁₃	Terpenoids	[M-H]-	Oleanolic acid-3-O-xylosyl(1→3)glucuronide
21	9.29	C ₃₀ H ₄₈ O ₄	Terpenoid	[M-H]-	2-Hydroxyoleanolic acid

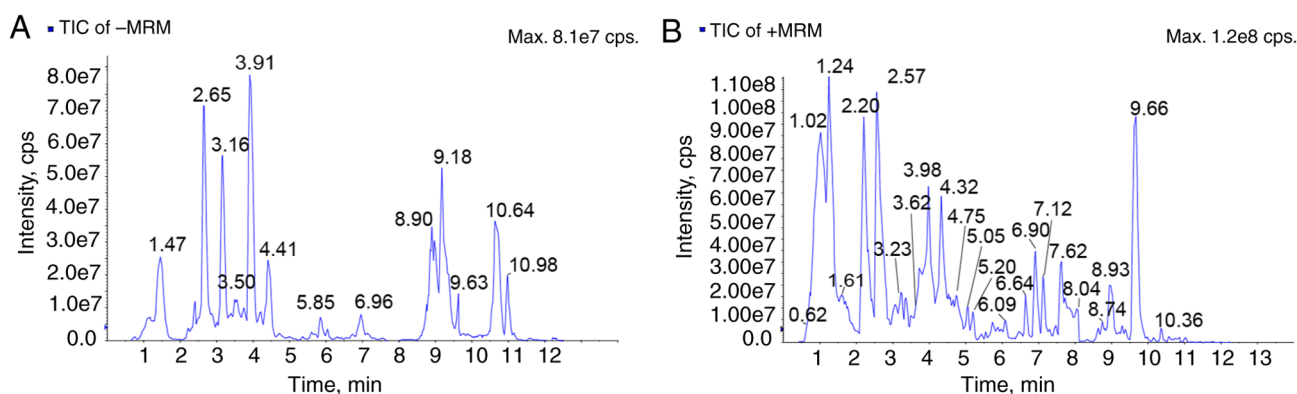


Figure 1. Total ion chromatogram of mass spectrometry analysis. (A) Negative ion mode. (B) Positive ion mode.

sections (Fig. 3A and B). Compared with the control group, the protein expression levels of CD31 and VEGF in the model and vehicle groups were significantly increased. However, CD31 and VEGF expression levels were significantly reduced in treatment groups compared with the model group. Moreover, this reduction was more pronounced as the drug concentration increased.

EAF inhibits the proliferation and migration of synovial cells and promotes apoptosis. To determine the effects of EAF on the synovium in RA, the effects of EAF on the proliferation, apoptosis and migration of HFLS-RAs were investigated. Results of the present study are displayed in Fig. 4. Following

24 and 48 h EAF treatment, results of the CCK-8 assay demonstrated that cell viability decreased following increases in EAF concentration, in a dose-dependent manner (Fig. 4A). Moreover, following 48 h drug treatment, the cell shape became round and wrinkled as the drug concentration increased (Fig. 4B). Results of the colony formation assay highlighted the inhibitory effects of EAF on cell proliferation. Notably, colony formation was significantly reduced in the treated groups compared with the control group and EAF reduced colony formation of HFLS-RAs in a dose-dependent manner (Fig. 4C). Results of the flow cytometry analysis demonstrated that EAF induced the apoptosis of HFLS-RAs (Fig. 4D). Moreover, cell migration was determined using

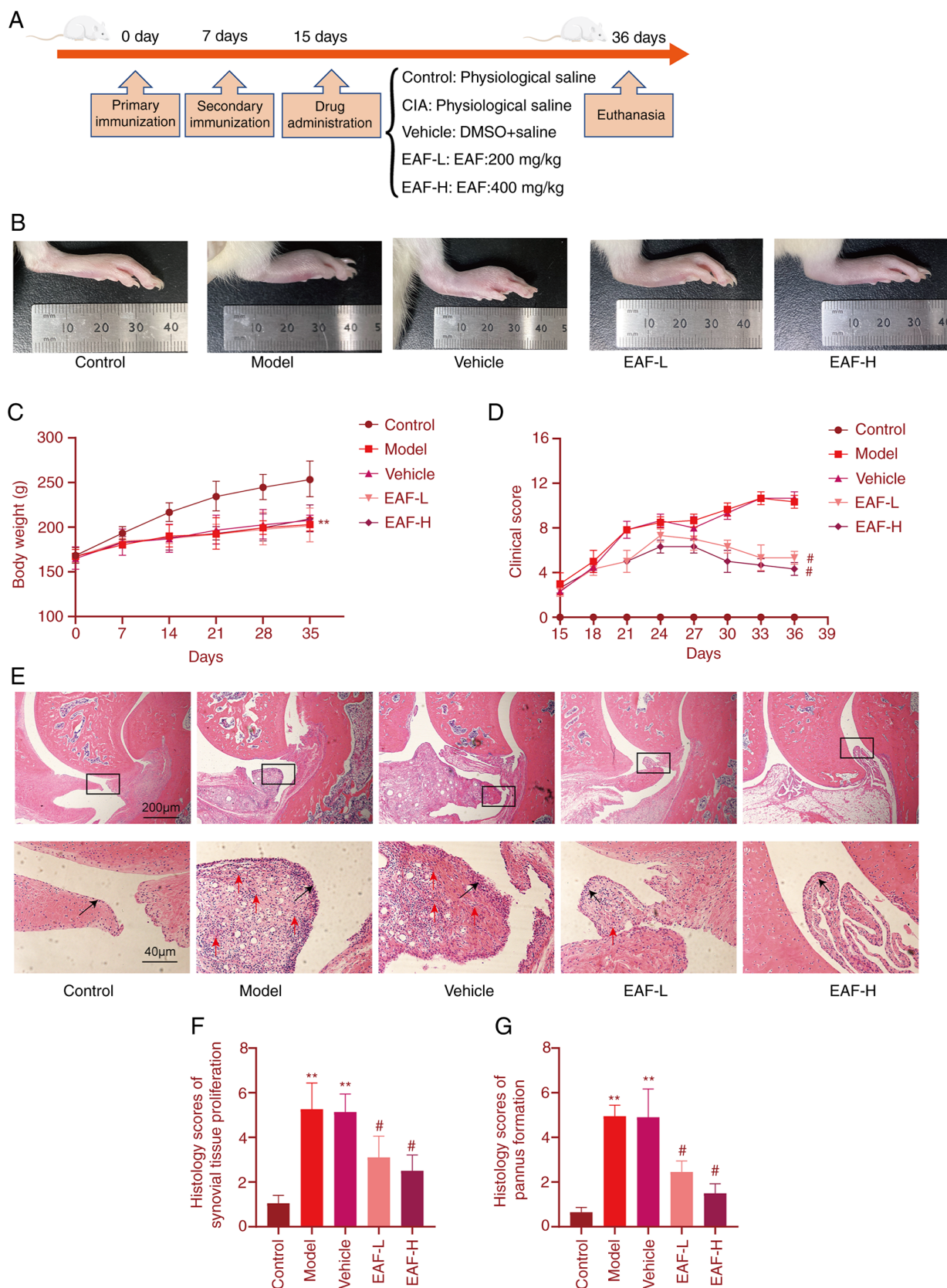


Figure 2. EAF treatment in CIA rats. (A) Time course of immunization and drug treatment in the CIA rat model. (B) Representative image of the right hindlimb of a CIA rat following 21 days of EAF treatment. (C) Body weight of CIA rats was recorded every seven days. (D) CIA rat limbs were clinically scored every 3 days. 0, without redness and swelling; 1, localized redness or swelling (wrist/ankle); 2, swelling or redness expanded to palm or sole; 3, redness and swelling in all joints; and 4, skin bursting/joint dysfunction or distortion. (E) Representative images of hematoxylin and eosin staining of CIA rat ankle joint sections (magnification, x40). Representative image of synovial tissue (local magnification, x200). (F) Histological score of synovial hyperplasia in each group. (G) Pannus formation score of synovial tissue in each group. ** $P < 0.01$ vs. control group, # $P < 0.01$ vs. model group. EAF, ethanol extract of *Anemone flaccida* Fr. Schmidt; CIA, collagen-induced arthritis; Control, blank control group; model, CIA group; vehicle, DMSO with saline group; EAF-L, low dose of ethanol extract of *Anemone flaccida* Fr. Schmidt group (200 mg/kg/day); and EAF-H, high dose ethanol extract of *Anemone flaccida* Fr. Schmidt group (400 mg/kg/day).

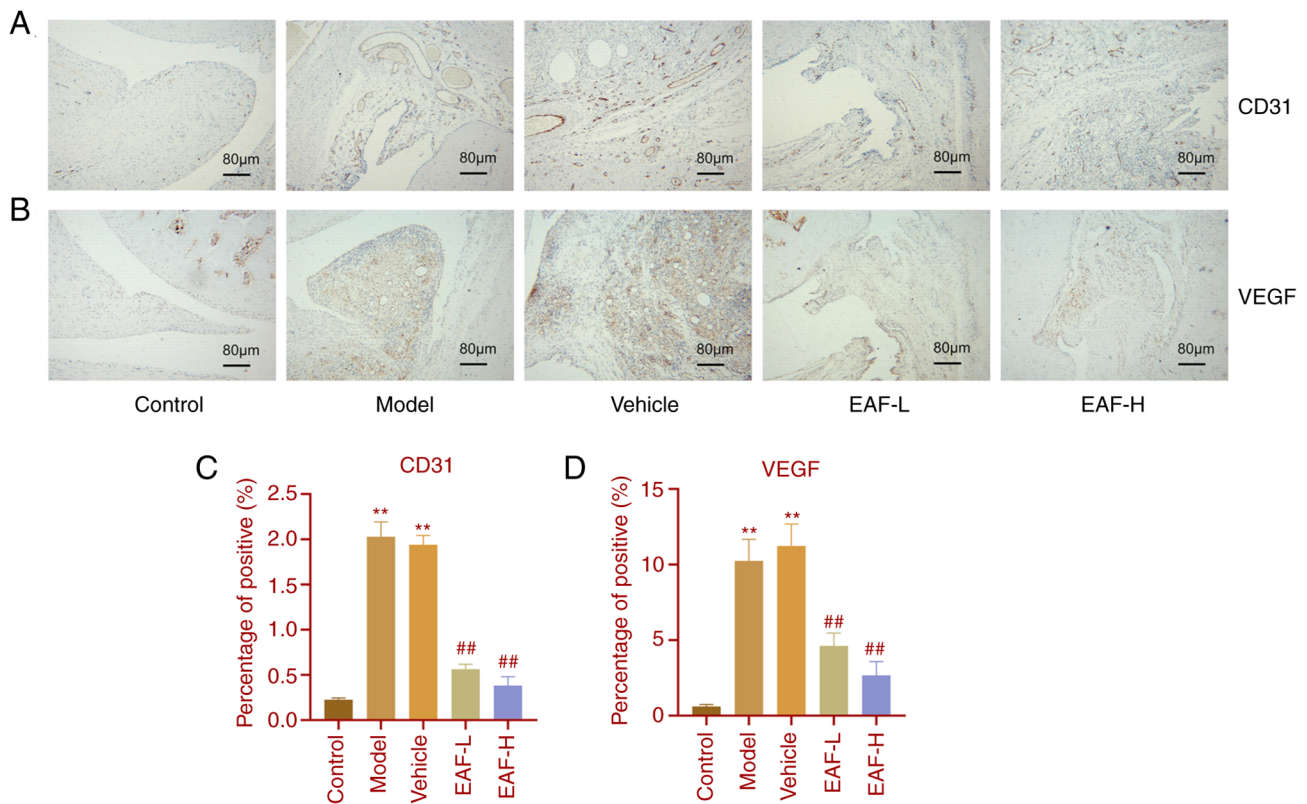


Figure 3. EAF inhibits angiogenesis and reduces the protein expression of VEGF in the synovial tissues of CIA rats. Immunohistochemical staining of (A) CD31 and (B) VEGF in CIA rat ankle joint sections. Quantitative analysis of immunohistochemical staining of (C) CD31 and (D) VEGF in synovial tissue. ## $P < 0.01$ vs. model group, ** $P < 0.01$ vs. control group. EAF, ethanol extract of *Anemone flaccida* Fr. Schmidt; CIA, collagen-induced arthritis; Control, blank control group; model, CIA group; vehicle, DMSO with saline group; EAF-L, low dose of ethanol extract of *Anemone flaccida* Fr. Schmidt group (200 mg/kg/day); and EAF-H, high dose ethanol extract of *Anemone flaccida* Fr. Schmidt group (400 mg/kg/day).

wound healing and Transwell assays. Results of the present study demonstrated that migration was significantly inhibited following treatment with EAF in a dose-dependent manner. Following 24 h EAF treatment, HFLS-RA migration was significantly reduced (Fig. 4E and F).

EAF inhibits VEGF-induced angiogenesis in vitro and in vivo. To further explore the effects of EAF on angiogenesis, VEGF was used as a positive control in the CAM model (Fig. 5A). Results of the present study demonstrated that blood vessels in the CAM in the VEGF group were significantly increased compared with those in the control group and blood vessels were distributed in a spoke-like shape with a sponge-like center. In the VEGF + EAF group, EAF inhibited the promoting effects of VEGF on blood vessels and the density of blood vessels was significantly lower than that in the VEGF group. However, there was no significant difference compared with the control group. Following EAF treatment alone, angiogenesis was significantly inhibited and blood vessel density was significantly reduced compared with the control group (Fig. 5B).

HUVECs were used to explore the effects of EAF on angiogenesis *in vitro* and results of the CCK-8 analysis demonstrated that EAF inhibited the viability of HUVECs in a dose-dependent manner. This inhibitory effect was more pronounced from 24 to 48 h of treatment (Fig. 5C). Results of the Transwell assay demonstrated that VEGF significantly increased the migration of HUVECs; however, treatment with

EAF inhibited this effect. In the EAF + VEGF group, cell migration was significantly lower than that in the VEGF and control groups and this inhibitory effect was more pronounced in the EAF group (Fig. 5E). In addition, VEGF significantly increased the number of endothelial cells forming tubules compared with the control group (Fig. 5D and F). However, following treatment with EAF + VEGF, the number of endothelial cells forming tubules was significantly reduced compared with the control group. Following treatment with EAF alone, few microtubules were formed.

EAF inhibits VEGFR signaling in HUVECs. The expression of cellular proteins was determined in HUVECs following EAF treatment. The present study first demonstrated that EAF exhibited a significant inhibitory effect on VEGF-induced cell migration and angiogenesis; thus, VEGFR-related signaling pathways were investigated further. Following the addition of VEGF in the cell culture, VEGFR expression levels and the phosphorylation of PI3K and AKT, were increased in HUVECs (Fig. 6A and B). However, EAF treatment eliminated this effect and the expression of VEGFR in the EAF + VEGF group was significantly lower than that in the VEGF and control groups. Notably, there was no significant difference in the phosphorylation of PI3K and AKT between EAF + VEGF and control groups; however, phosphorylation was significantly lower than that in the VEGF group. In addition, following treatment with EAF alone, phosphorylation of PI3K and AKT was significantly lower than that in the control and

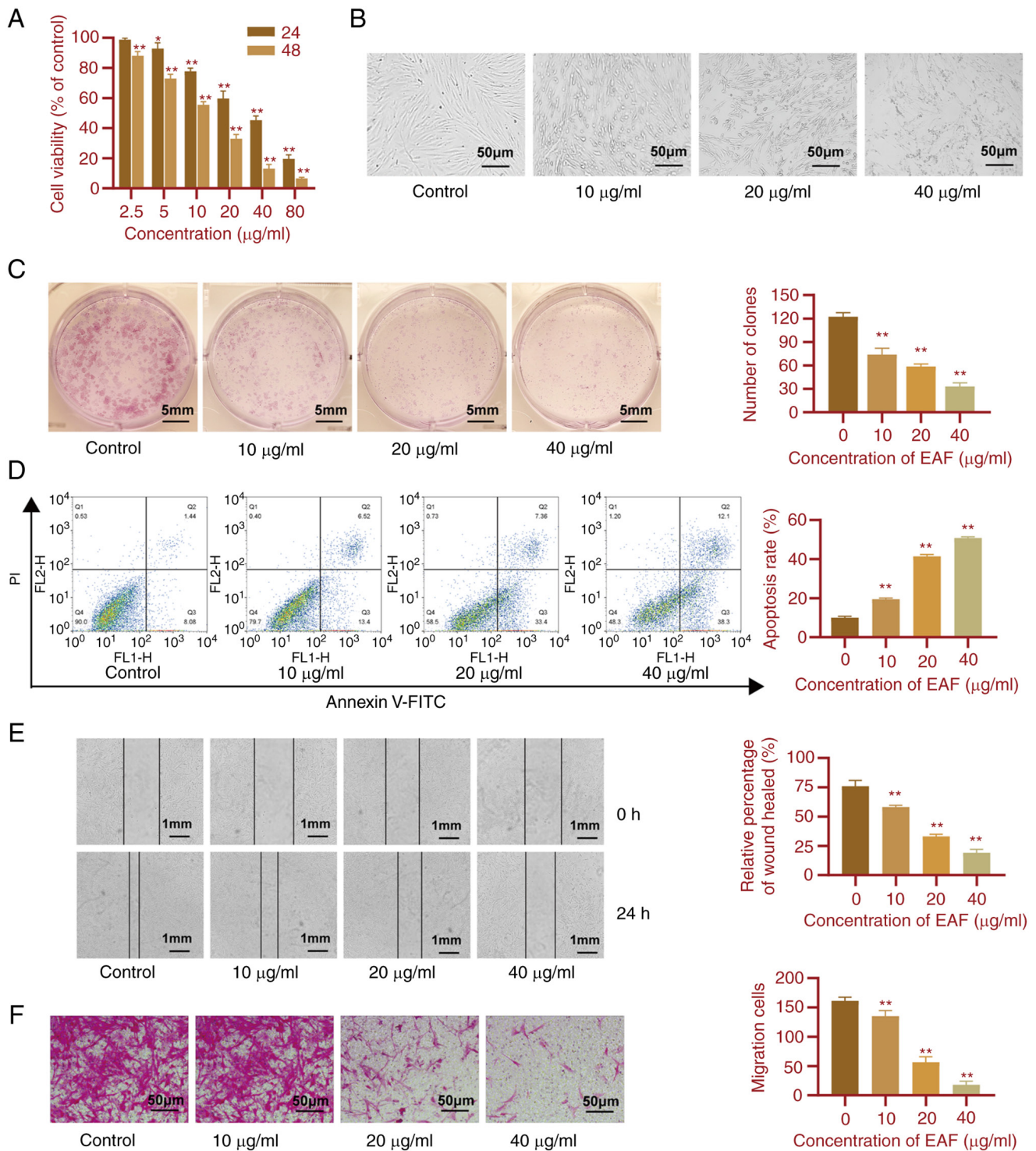


Figure 4. EAF inhibits the proliferation and migration of synovial cells and promotes apoptosis. (A) Viability of HFLS-RAs detected using a Cell Counting Kit-8 assay following treatment with EAF for 24 or 48 h. (B) Images of HFLS-RAs following treatment with different concentrations of EAF for 48 h. (C) Colony formation of HFLS-RAs following treatment with EAF. (D) Apoptosis of HFLS-RAs following treatment with different concentrations of EAF for 24 h was detected using flow cytometry. (E) Wound healing assay was used to detect the migration of HFLS-RAs following treatment with different concentrations of EAF. (F) Images of migrated HFLS-RAs following treatment with different concentrations of EAF. Data are expressed as the mean \pm standard deviation. Experiments were carried out at least three times. * $P < 0.05$, ** $P < 0.01$ vs. control group. EAF, ethanol extract of *Anemone flaccida* Fr. Schmidt; HFLS-RAs, human fibroblast-like synoviocytes-RA.

VEGF groups. Protein expression levels of p-mTOR were not significantly increased in the VEGF group compared with the control group; however, these were significantly decreased in the EAF + VEGF and EAF groups, compared with the control and VEGF groups.

Discussion

The present study aimed to explore the effects and mechanisms of EAF in the treatment of RA and revealed the inhibitory effects on synovial proliferation and angiogenesis.

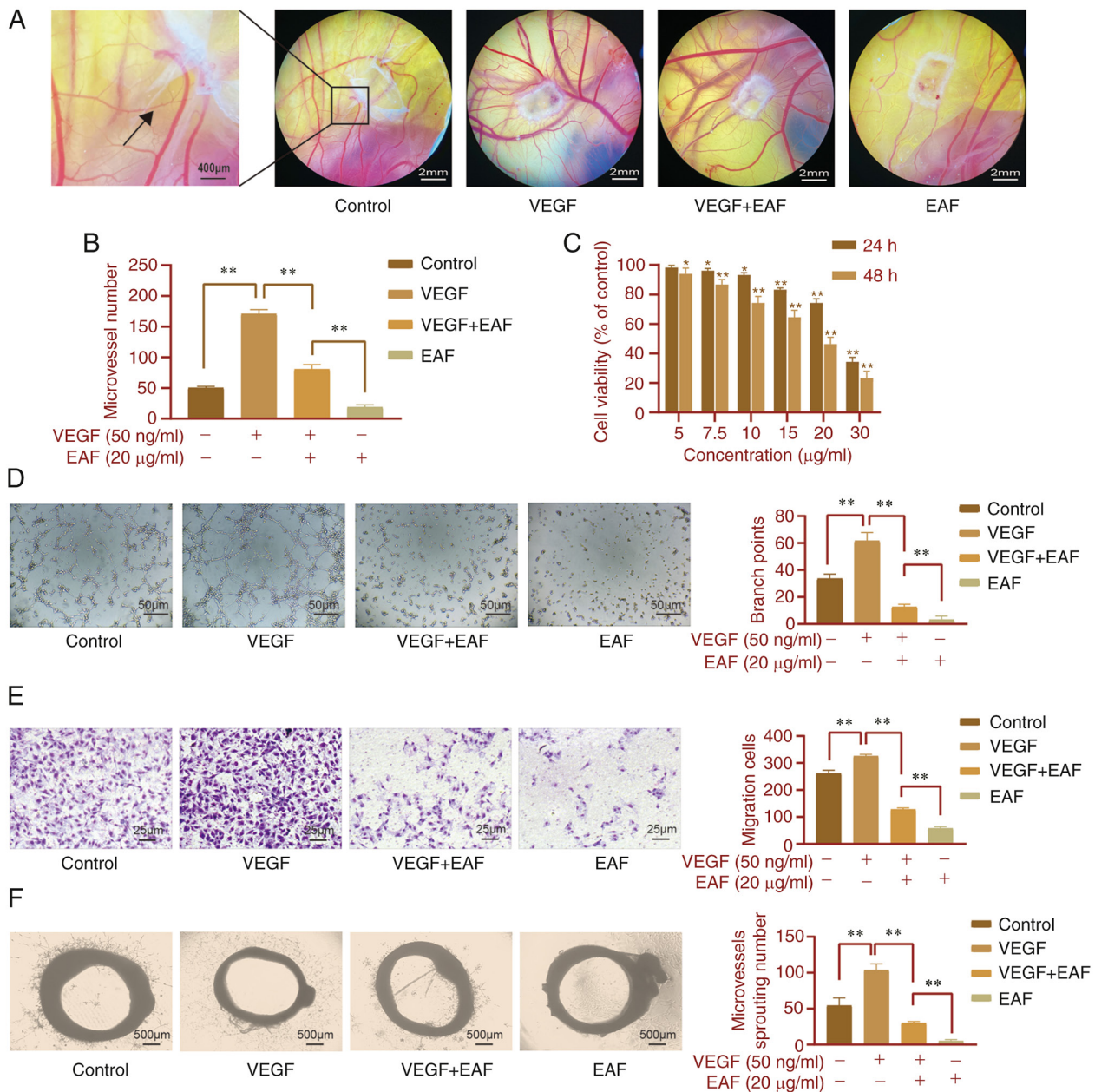


Figure 5. EAF inhibits VEGF-induced angiogenesis *in vitro* and *in vivo*. (A) CAM analysis demonstrated the distribution of microvessels surrounding the gelatin sponge, containing EAF and/or VEGF. The black arrow indicates microvessels in the locally magnified image. (B) Statistical analysis of the number of microvessels. (C) HUVEC viability was detected using a Cell Counting Kit-8 assay following treatment with EAF for 24 or 48 h. (D) Tube formation of HUVECs following treatment with EAF and/or VEGF. (E) Migration of HUVECs following treatment with different concentrations of EAF and/or VEGF. (F) Aortic ring angiogenesis was inhibited following treatment with EAF and/or VEGF. Data are presented as the mean \pm standard deviation. Experiments were carried out at least three times. * $P < 0.05$, ** $P < 0.01$ vs. control group. EAF, ethanol extract of *Anemone flaccida* Fr. Schmidt; CAM, chick chorioallantois membrane; HUVEC, human umbilical vein endothelial cells.

It provided a novel theoretical basis for the clinical use of *Anemone flaccida* Fr. Schmidt.

Liu *et al* (20) demonstrated that triterpenoid saponins, the main components of *Anemone flaccida*, significantly improved the joint inflammatory response in arthritic mice and significantly inhibited lipopolysaccharide-induced TNF- α expression in RAW264.7 cells. Results of a previous study demonstrated that *Anemone flaccida* Fr. Schmidt significantly increased bone mineral density, bone volume fraction and trabecular thickness in arthritic mice and reduced trabecular separation in periarticular and extraarticular inflamed joints (21). *Anemone flaccida* Fr. Schmidt is effective in the

treatment of RA; however, to the best of the authors' knowledge, no studies have reported the specific effects on the RA synovium. Consistent with the results of previous studies, results of the present study demonstrated that the main components of the ethanolic extract included flavonoids and phenolic acids. Moreover, results of the present study demonstrated the inhibitory effects of EAF on intra-articular synovial membrane proliferation and angiogenesis in RA, both *in vitro* and *in vivo*.

The therapeutic effects of EAF on RA were investigated using a CIA model in the present study. Compared with the model group, EAF markedly improved joint redness and

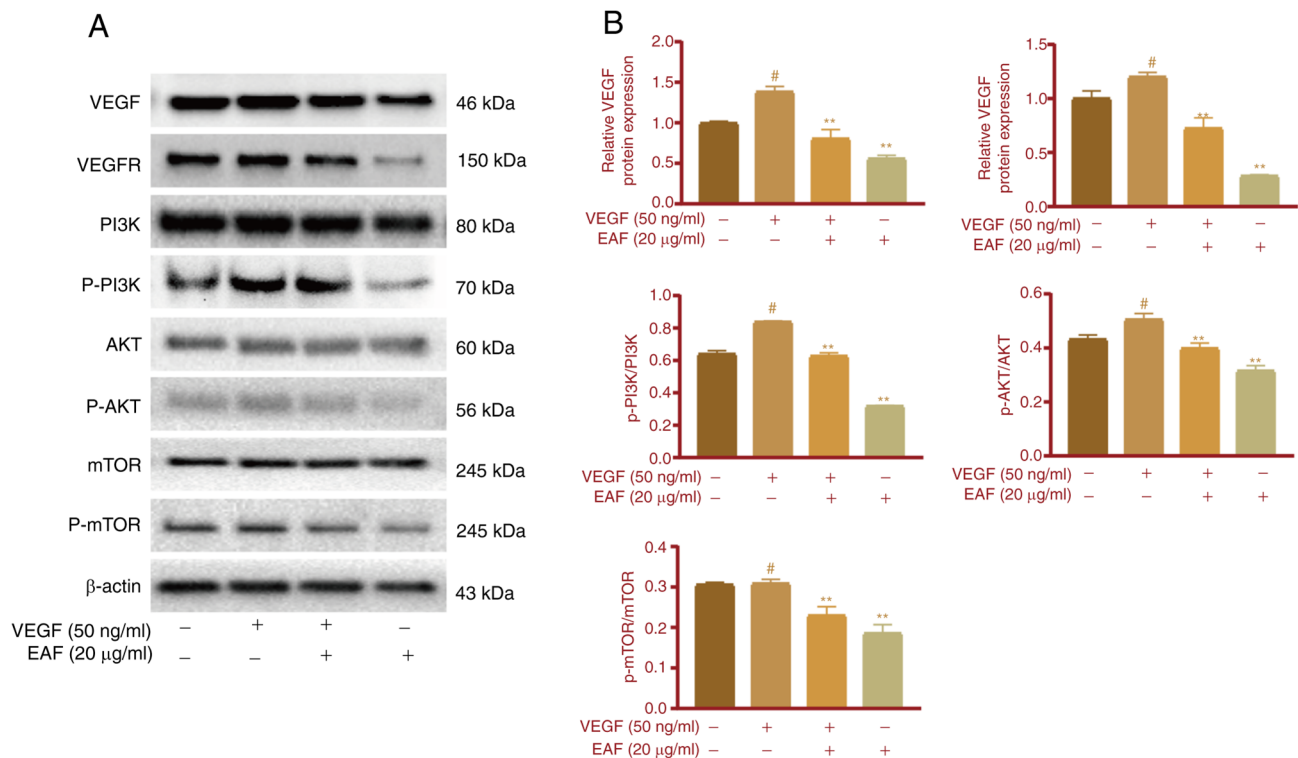


Figure 6. Effects of EAF and/or VEGF on the VEGFR-PI3K-AKT-mTOR pathway in HUVECs. (A) Representative western blots demonstrating the components of the VEGFR-PI3K-AKT-mTOR pathway, following treatment with EAF and/or VEGF in HUVECs. (B) Quantitative analysis of the western blots following treatment with EAF and/or VEGF in HUVECs. Data are expressed as mean \pm standard deviation. Experiments were carried out at least three times. [#]P<0.05 vs. control group, ^{**}P<0.01 vs. positive control group (VEGF). EAF, ethanol extract of *Anemone flaccida* Fr. Schmidt; HUVEC, human umbilical vein endothelial cells; p-, phosphorylated.

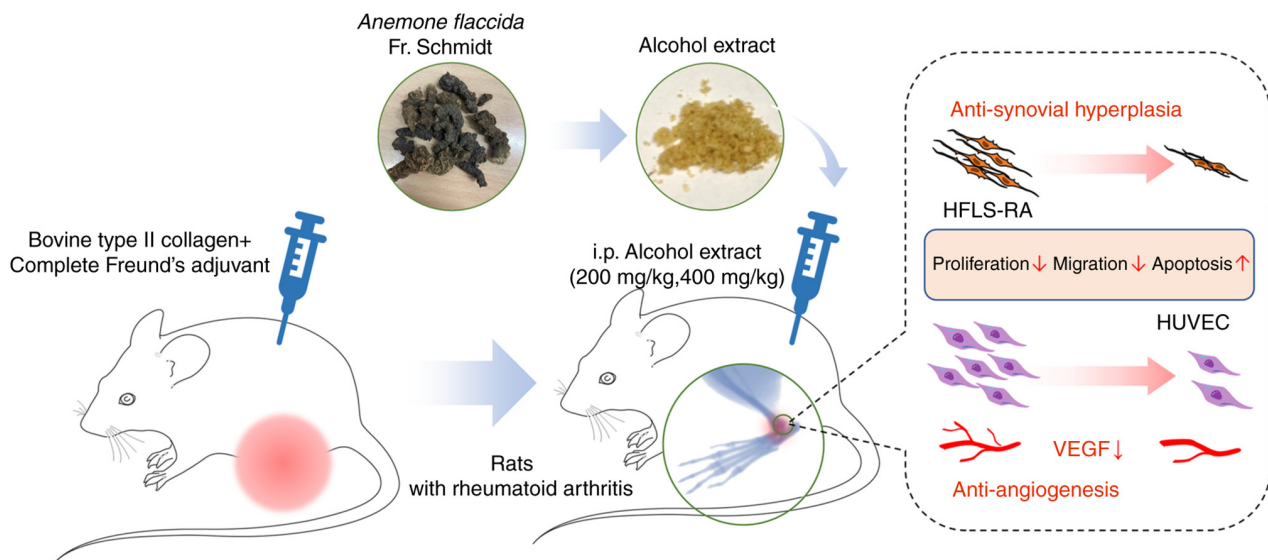


Figure 7. EAF may treat RA through inhibition of synovial hyperplasia and angiogenesis. EAF, ethanol extract of *Anemone flaccida* Fr. Schmidt; HFLS, human fibroblast-like synoviocytes; RA, rheumatoid arthritis; HUVEC, human umbilical vein endothelial cells.

swelling in CIA model rats. Notably, the body weight of CIA model rats was significantly lower than that of the control group, which may have been due to a reduction in food intake as a result of arthralgia. There was no significant difference in body weight between the model group and the EAF-treated group, which may demonstrate that EAF did not induce weight loss. Subsequent immunohistochemical and H&E staining

analyses demonstrated significant improvements in synovial tissue proliferation and inhibition of neovascularization in RA, following treatment with EAF. Thus, it was hypothesized that EAF may aid in the treatment of RA via inhibition of rheumatoid synovial cells and angiogenesis.

Fibroblast-like synoviocytes are derived from mesenchymal stem cells, rich in rough endoplasmic reticulum, and

are the main component of synovial tissue (22,23). Synovial fibroblasts exert a variety of pathological changes in RA through the secretion of inflammatory factors, including inflammatory infiltration, synovial proliferation and vascular opacification formation, mediating pathways that play an important role in cartilage destruction and joint deformation (24,25). Results of previous studies demonstrate that activated synovial cells exhibit properties comparable with tumor-like cells, such as excessive proliferation, migration and insufficient apoptosis (26,27). RA-FLS destroys cartilage and bone through migration and invasion, promoting the progression of arthritis (28). Thus, targeting RA-FLSs to modulate the aggressiveness or apoptosis of FLS cells may be a novel therapeutic approach for RA (29,30). The results of the present study demonstrated that EAF significantly inhibited the viability of HFLS-RAAs, suppressed the proliferation, migration and invasion and promoted apoptosis in a dose-dependent manner.

Neovascularization plays a key role in synovial development in the inflammatory microenvironment of RA (31). Vascular endothelial cells respond to various inflammatory and growth factors in RA and maintain proliferation in the synovium through proliferating and migrating to form new blood vessels (32). The results of a previous study demonstrated that levels of pro-angiogenic factors in the RA synovium, including VEGF and platelet derived growth factor (PDGF), respond to the severity of RA and therapy (33). In the present study, both neovascularization and VEGF expression were significantly reduced in the synovial membrane of CIA rats treated with EAF. Thus, it was hypothesized that EAF inhibited synovial angiogenesis and improved arthritic symptoms through suppression of VEGF expression. A CAM model was established and VEGF-165 was added to simulate the VEGF-rich environment in arthritis. The results of the present study demonstrated that VEGF-165 significantly stimulated angiogenesis in the CAM model; however, EAF also inhibited angiogenesis in the presence of VEGF-165. The inhibitory effects of EAF on VEGF-activated endothelial cell migration and tube formation were examined and results of the present study demonstrated that EAF markedly inhibited the migration and tube formation of HUVECs. These results were also observed in the presence of VEGF-165.

Angiogenesis occurs through endothelial cell proliferation, differentiation, migration and lumen formation (34). Notably, VEGF is a key regulatory factor of angiogenesis (35,36). VEGF also plays a role in the vascular proliferation and blood vessel invasion of the synovial lining membrane in RA (37). The binding of VEGF to its receptor VEGFR activates the PI3K/AKT signaling pathway, which, in turn, regulates endothelial cell formation of blood vessels (38). Results of previous studies demonstrated that triterpene saponins markedly inhibit the PI3K/AKT signaling pathway (39,40). Notably, results of the present study demonstrated that treatment with VEGF-165 activated the PI3K/AKT signaling pathway and HUVEC migration and tube formation were significantly increased. However, these effects were reversed following EAF treatment.

In conclusion, results of the present study demonstrated that EAF exerted notable effects on RA. EAF markedly inhibited synovial proliferation and angiogenesis in arthritic joints and this was associated with regulation of the VEGFR/PI3K/AKT signaling pathway (Fig. 7). These findings further revealed the

anti-RA mechanism of EAF and provided a novel theoretical basis for its clinical application. In addition, the anti-angiogenesis effects of EAF should be further explored in tumors.

Acknowledgements

Not applicable.

Funding

The present study was supported by the Chinese Academy of Medical Sciences (CAMS) Innovation Fund for Medical Sciences (grant no. 2018-I2M-AI-015) and the National Science Foundation of China (grant no. 81702920).

Availability of data and materials

The datasets used and/or analyzed during the current study are available from the corresponding author on reasonable request.

Authors' contributions

GZ, DYC and QR designed the study, conceived the experiments, outlined the experimental scheme, confirmed the authenticity of all the raw data and revised the manuscript. QR, HY and XZ performed the experiments and drafted the manuscript. FHW, XHG and YDX analyzed the experimental data. GZ, QR, FHW, XHG and YDX reviewed and edited the manuscript. All authors read and approved the final manuscript.

Ethics approval and consent to participate

The animal experiments were carried following approval by the Laboratory Animal Ethics Committee of Hubei Academy of Chinese Medicine Sciences (approval no. 202208001).

Patient consent for publication

Not applicable.

Competing interests

The authors declare that they have no competing interests.

Reference

1. Sparks JA: Rheumatoid arthritis. *Ann Intern Med* 170: ITC1-ITC16, 2019.
2. Aletaha D and Smolen JS: Diagnosis and management of rheumatoid arthritis: A review. *JAMA* 320: 1360-1372, 2018.
3. Smith MH and Berman JR: What is rheumatoid arthritis? *Jama* 327: 1194, 2022.
4. van der Woude D and van der Helm-van Mil AHM: Update on the epidemiology, risk factors, and disease outcomes of rheumatoid arthritis. *Best Pract Res Clin Rheumatol* 32: 174-187, 2018.
5. You S, Koh JH, Leng L, Kim WU and Bucala R: The tumor-like phenotype of rheumatoid synovium: Molecular profiling and prospects for precision medicine. *Arthritis Rheumatol* 70: 637-652, 2018.
6. Cush JJ: Rheumatoid arthritis: Early diagnosis and treatment. *Med Clin North Am* 105: 355-365, 2021.
7. Kim JW, Kong JS, Lee S, Yoo SA, Koh JH, Jin J and Kim WU: Angiogenic cytokines can reflect the synovitis severity and treatment response to biologics in rheumatoid arthritis. *Exp Mol Med* 52: 843-853, 2020.

8. Radu AF and Bungau SG: Management of rheumatoid arthritis: An overview. *Cells* 10: 2857, 2021.
9. Abbasi M, Mousavi MJ, Jamalzehi S, Alimohammadi R, Bezvan MH, Mohammadi H and Aslani S: Strategies toward rheumatoid arthritis therapy; the old and the new. *J Cell Physiol* 234: 10018-10031, 2019.
10. Burmester GR and Pope JE: Novel treatment strategies in rheumatoid arthritis. *Lancet* 389: 2338-2348, 2017.
11. Yu H, Qiu Y, Tasneem S, Daniyal M, Li B, Cai X, Rahman AU and Wang W: Advancement of natural compounds as anti-rheumatoid arthritis agents: A focus on their mechanism of actions. *Mini Rev Med Chem* 21: 2957-2975, 2021.
12. Wang Y, Chen S, Du K, Liang C, Wang S, Boadi EO, Li J, Pang X, He J and Chang YX: Traditional herbal medicine: Therapeutic potential in rheumatoid arthritis. *J Ethnopharmacol* 279: 114368, 2021.
13. Liu Q, Zhu XZ, Feng RB, Liu Z, Wang GY, Guan XF, Ou GM, Li YL, Wang Y, Li MM and Ye WC: Crude triterpenoid saponins from *Anemone flaccida* (Di Wu) exert anti-arthritis effects on type II collagen-induced arthritis in rats. *Chin Med* 10: 20, 2015.
14. Liu C, Yang Y, Sun D, Wang C, Wang H, Jia S, Liu L and Lin N: Total saponin from *Anemone flaccida* fr. Schmidt prevents bone destruction in experimental rheumatoid arthritis via inhibiting osteoclastogenesis. *Rejuvenation Res* 18: 528-542, 2015.
15. Linghu KG, Xiong SH, Zhao GD, Zhang T, Xiong W, Zhao M, Shen XC, Xu W, Bian Z, Wang Y and Yu H: *Sigesbeckia orientalis* L. Extract alleviated the collagen type II-induced arthritis through inhibiting multi-target-mediated synovial hyperplasia and inflammation. *Front Pharmacol* 11: 547913, 2020.
16. Hawkins P, Armstrong R, Boden T, Garside P, Knight K, Lilley E, Seed M, Wilkinson M and Williams RO: Applying refinement to the use of mice and rats in rheumatoid arthritis research. *Inflammopharmacology* 23: 131-150, 2015.
17. Rao Q, Li R, Yu H, Xiang L, He B, Wu F and Zhao G: Effects of dihydroartemisinin combined with cisplatin on proliferation, apoptosis and migration of HepG2 cells. *Oncol Lett* 24: 275, 2022.
18. Hao DC, Gu X and Xiao P: *Anemone* medicinal plants: Ethnopharmacology, phytochemistry and biology. *Acta Pharm Sin B* 7: 146-158, 2017.
19. Zhao L, Chen WM and Fang QC: Triterpenoid Saponins from *Anemone flaccida*. *Planta Med* 56: 92-93, 1990.
20. Liu Q, Xiao XH, Hu LB, Jie HY, Wang Y, Ye WC, Li MM and Liu Z: Anhuienoside C ameliorates collagen-induced arthritis through inhibition of MAPK and NF- κ B signaling pathways. *Front Pharmacol* 8: 299, 2017.
21. Kong X, Wu W, Yang Y, Wan H, Li X, Zhong M, Zhao H, Su X, Jia S, Ju D and Lin N: Total saponin from *Anemone flaccida* Fr. Schmidt abrogates osteoclast differentiation and bone resorption via the inhibition of RANKL-induced NF- κ B, JNK and p38 MAPKs activation. *J Transl Med* 13: 91, 2015.
22. Németh T, Nagy G and Pap T: Synovial fibroblasts as potential drug targets in rheumatoid arthritis, where do we stand and where shall we go? *Ann Rheum Dis* 81: 1055-1064, 2022.
23. Zhai KF, Duan H, Cui CY, Cao YY, Si JL, Yang HJ, Wang YC, Cao WG, Gao GZ and Wei ZJ: Liquiritin from glycyrrhiza uralensis attenuating rheumatoid arthritis via reducing inflammation, suppressing angiogenesis, and inhibiting MAPK signaling pathway. *J Agric Food Chem* 67: 2856-2864, 2019.
24. Nygaard G and Firestein GS: Restoring synovial homeostasis in rheumatoid arthritis by targeting fibroblast-like synoviocytes. *Nat Rev Rheumatol* 16: 316-333, 2020.
25. Falconer J, Murphy AN, Young SP, Clark AR, Tiziani S, Guma M and Buckley CD: Review: Synovial cell metabolism and chronic inflammation in rheumatoid arthritis. *Arthritis Rheumatol* 70: 984-999, 2018.
26. Zhang Q, Liu J, Zhang M, Wei S, Li R, Gao Y, Peng W and Wu C: Apoptosis induction of fibroblast-like synoviocytes is an important molecular-mechanism for herbal medicine along with its active components in treating rheumatoid arthritis. *Biomolecules* 9: 795, 2019.
27. Du H, Zhang X, Zeng Y, Huang X, Chen H, Wang S, Wu J, Li Q, Zhu W, Li H, *et al.*: A novel phytochemical, DIM, inhibits proliferation, migration, invasion and TNF- α induced inflammatory cytokine production of synovial fibroblasts from rheumatoid arthritis patients by targeting MAPK and AKT/mTOR signal pathway. *Front Immunol* 10: 1620, 2019.
28. You S, Yoo SA, Choi S, Kim JY, Park SJ, Ji JD, Kim TH, Kim KJ, Cho CS, Hwang D and Kim WU: Identification of key regulators for the migration and invasion of rheumatoid synoviocytes through a systems approach. *Proc Natl Acad Sci USA* 111: 550-555, 2014.
29. Hu P, Dong ZS, Zheng S, Guan X, Zhang L, Li L and Liu Z: The effects of miR-26b-5p on fibroblast-like synovial cells in rheumatoid arthritis (RA-FLS) via targeting EZH2. *Tissue Cell* 72: 101591, 2021.
30. Svensson MND, Zoccheddu M, Yang S, Nygaard G, Secchi C, Doody KM, Slowikowski K, Mizoguchi F, Humby F, Hands R, *et al.*: Synoviocyte-targeted therapy synergizes with TNF inhibition in arthritis reversal. *Sci Adv* 6: eaba4353, 2020.
31. Le THV and Kwon SM: Vascular endothelial growth factor biology and its potential as a therapeutic target in rheumatic diseases. *Int J Mol Sci* 22: 5387, 2021.
32. Baggio C, Boscaro C, Oliviero F, Trevisi L, Ramaschi G, Ramonda R, Bolego C and Cignarella A: Gender differences and pharmacological regulation of angiogenesis induced by synovial fluids in inflammatory arthritis. *Biomed Pharmacother* 152: 113181, 2022.
33. Balogh E, Pusztai A, Hamar A, Végh E, Szamosi S, Kerekes G, McCormick J, Biniecka M, Szántó S, Szűcs G, *et al.*: Autoimmune and angiogenic biomarkers in autoimmune atherosclerosis. *Clin Immunol* 199: 47-51, 2019.
34. Sajib S, Zahra FT, Lionakis MS, German NA and Mikelis CM: Mechanisms of angiogenesis in microbe-regulated inflammatory and neoplastic conditions. *Angiogenesis* 21: 1-14, 2018.
35. Li Y, Liu Y, Wang C, Xia WR, Zheng JY, Yang J, Liu B, Liu JQ and Liu LF: Succinate induces synovial angiogenesis in rheumatoid arthritis through metabolic remodeling and HIF-1 α /VEGF axis. *Free Radic Biol Med* 126: 1-14, 2018.
36. MacDonald IJ, Liu SC, Su CM, Wang YH, Tsai CH and Tang CH: Implications of angiogenesis involvement in arthritis. *Int J Mol Sci* 19: 2012, 2018.
37. Malemud CJ: Growth hormone, VEGF and FGF: Involvement in rheumatoid arthritis. *Clin Chim Acta* 375: 10-19, 2007.
38. Wang X, Bove AM, Simone G and Ma B: Molecular bases of VEGFR-2-mediated physiological function and pathological role. *Front Cell Dev Biol* 8: 599281, 2020.
39. Liu X, Mi X, Wang Z, Zhang M, Hou J, Jiang S, Wang Y, Chen C and Li W: Ginsenoside Rg3 promotes regression from hepatic fibrosis through reducing inflammation-mediated autophagy signaling pathway. *Cell Death Dis* 11: 454, 2020.
40. Jang E and Lee JH: Promising anticancer activities of alismatis rhizome and its triterpenes via p38 and PI3K/Akt/mTOR signaling pathways. *Nutrients* 13: 2455, 2021.



This work is licensed under a Creative Commons Attribution-NonCommercial-NoDerivatives 4.0 International (CC BY-NC-ND 4.0) License.